

Infrared Probe of Itinerant Ferromagnetism in $\text{Ga}_{1-x}\text{Mn}_x\text{As}$

E. J. Singley,¹ R. Kawakami,² D. D. Awschalom,² and D. N. Basov¹

¹*Department of Physics, University of California, San Diego, California 92093-0319*

²*Department of Physics, University of California, Santa Barbara, California 93106*

(Received 15 May 2002; published 9 August 2002)

The doping and temperature dependence of the complex conductivity is determined for the ferromagnetic semiconductor $\text{Ga}_{1-x}\text{Mn}_x\text{As}$. A broad resonance develops with Mn doping at an energy scale of ~ 200 meV, well within the GaAs band gap. Possible origins of this feature are explored in the context of a Mn induced impurity band and intervalence band transitions. From a sum rule analysis of the conductivity data the effective mass of the itinerant charge carriers is found to be at least a factor of 3 greater than what is expected for hole doped GaAs. In the ferromagnetic state a significant decrease in the effective mass is observed, demonstrating the role played by the heavy carriers in inducing ferromagnetism in this system.

DOI: 10.1103/PhysRevLett.89.097203

PACS numbers: 75.50.Pp, 71.55.Eq, 78.20.-e

$\text{Ga}_{1-x}\text{Mn}_x\text{As}$ and other transition metal doped III-V materials are of great interest for both their potential technological importance and the fundamental novelty of a ferromagnetic semiconductor with $T_C \sim 100$ K [1,2]. It is generally believed that the ferromagnetism in these systems is carrier mediated. Currently there is no consensus on the gross features of the electronic structure of heavily doped $\text{Ga}_{1-x}\text{Mn}_x\text{As}$, and therefore the details of the itinerant ferromagnetic state are unresolved. A common picture that has been used to interpret both transport [3] and magnetoabsorption [4] experiments is that Mn dopes a hole into the GaAs valence band and also acts as a localized spin [5–7]. Within this view, the holes promoting ferromagnetism via Ruderman-Kittel-Kasuya-Yosida interaction ought to be strongly influenced by the spin-orbit interaction. However, the idea that the holes reside in the unperturbed GaAs valence band is not certain. Indeed, angle resolved photoemission spectroscopy [8] observes an impurity band near E_F . Infrared measurements of the absorption coefficient also reveal a strong resonance near the energy of the Mn acceptor level in GaAs [9]. Several scenarios of the ferromagnetic state rely on the existence of a well-defined impurity band with the Fermi energy (E_F) pinned inside this band [10]. Naturally, a detailed description of the ferromagnetic state will require a well-defined picture of the electronic structure which is lacking at the moment. Knowledge of the carriers' effective mass is also essential when considering spin and/or charge injection from $\text{Ga}_{1-x}\text{Mn}_x\text{As}$.

From spectroscopic measurements in the infrared we determine the complex conductivity, $\sigma(\omega) = \sigma_1(\omega) + i\sigma_2(\omega)$, with which we are able to address the issues raised above. An integration of the dissipative part of the conductivity, $\sigma_1(\omega)$, provides a measure of the itinerant carriers' mass which is a direct probe of the electronic band structure. From this analysis we estimated the effective mass to be $0.7m_e < m^* < 15m_e$ for the $x = 0.052$ sample, and larger at all other dopings, which suggest that the

carriers do not simply reside in the unaltered GaAs valence band. By additionally studying the temperature dependence of m^* we see a strong decrease below T_C providing direct support for itinerant carrier driven ferromagnetism.

Transmission, $T(\omega)$, and reflectance, $R(\omega)$, experiments were performed on thin films of $\text{Ga}_{1-x}\text{Mn}_x\text{As}$ grown with the low temperature molecular-beam epitaxy (LTMBE) method [11]. The series of films studied included a paramagnetic sample with $x = 0.017$, along with five ferromagnetic films with Mn concentration of $x = 0.028, 0.040, 0.052, 0.066,$ and 0.079 . The films had a thickness of $0.5 \mu\text{m}$, and were grown on single crystal GaAs substrates 0.5 mm thick. $T(\omega)$ measurements were performed between 5 and 292 K, well above and below the Curie temperature of the samples. The energy range covered in the experiment extends from 15 to $12\,000 \text{ cm}^{-1}$ (the band gap in GaAs). The complex conductivity was determined from both a combination of $T(\omega)$ and $R(\omega)$ measurements, and additionally from a Kramers-Kronig analysis of the $T(\omega)$ data [12].

The top panel of Fig. 1 shows $\sigma_1(\omega)$ for all the films throughout the measured frequency range at 292 K. The conductivity of the paramagnetic, $x = 0.017$ sample below 2500 cm^{-1} is very similar to that of undoped GaAs (grey line), with a magnitude of $\sim 5 \Omega^{-1} \text{ cm}^{-1}$, near the noise floor of the present experiment. At higher energies a strong broadening of the GaAs gap edge is observed in all samples. Such broadening can be attributed to As disorder caused by the low temperature epitaxial growth [14]. All ferromagnetic samples with $x \geq 0.028$ reveal new features in the data: (i) a strong resonance at $\omega \sim 2000 \text{ cm}^{-1}$ inside the gap of the GaAs host and (ii) finite conductivity in the dc limit signaling metallic transport (Figs. 1 and 2). The absence of the intragap absorption in the data for the paramagnetic $x = 0.017$ film suggests that this sample is fully compensated. Therefore, the onset of ferromagnetism in the $\text{Ga}_{1-x}\text{Mn}_x\text{As}$ series coincides with the appearance of the conducting carriers response in the intragap region.

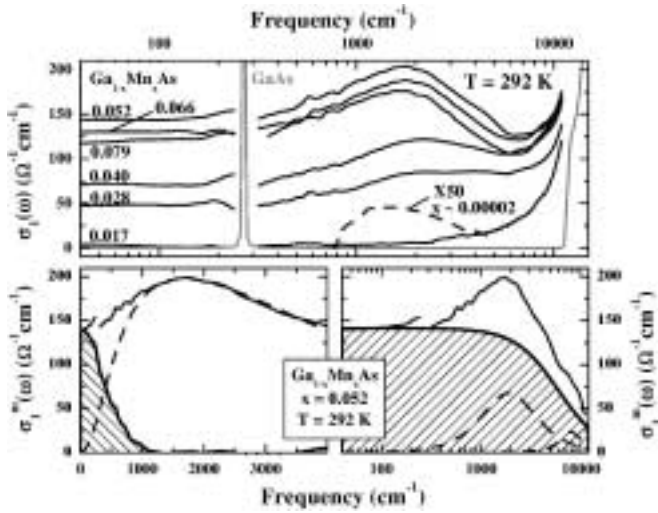


FIG. 1. Top panel: $\sigma_1(\omega)$ for all samples at $T = 292$ K. The gray line is the conductivity of undoped GaAs. All Mn doped samples show a substantial broadening of the GaAs gap edge, likely due to As disorder. Ferromagnetic samples also show a broad resonance near 2000 cm^{-1} . The dashed line corresponds to $\sigma_1(\omega)$ for a nonmagnetic, very dilute Mn concentration sample, where the absorption band is due to electronic transitions between the valence band and Mn acceptor level [13]. Bottom panels: Both panels show $\sigma_1^m(\omega)$ for the $x = 0.052$ sample at $T = 292$ K. Two different methods of separating the intraband and interband conductivity are demonstrated, as described in the text. Dashed lines in the right panel correspond to Eq. (2) with $\omega_{p,1}^2 = 1.7 \times 10^7$ cm^{-2} , $\omega_{o,1} = 1900$ cm^{-1} , $\Gamma_1 = 3200$ cm^{-1} , $\omega_{p,2}^2 = 7 \times 10^6$ cm^{-2} , $\omega_{o,2} = 8000$ cm^{-1} , $\Gamma_2 = 5000$ cm^{-1} , while the thick line is determined from Eq. (2) with $\omega_{p,D}^2 = 5.1 \times 10^7$ cm^{-2} , $\omega_{o,D} = 0$ cm^{-1} , $\Gamma_D = 6000$ cm^{-1} . The dashed line in the left panel is a single Lorentz oscillator [Eq. (2)] with $\omega_p^2 = 6 \times 10^7$ cm^{-2} , $\omega_o = 1675$ cm^{-1} , $\Gamma = 5050$ cm^{-1} . The thick lines with shading underneath are different estimates of the intraband conductivity used to determine a likely range of the carrier mass.

LTMBE grown GaAs is naturally n -type [15], so excessive Mn is required to dope holes into the system. Postgrowth annealing has been shown to affect the magnetic and electrical properties of $\text{Ga}_{1-x}\text{Mn}_x\text{As}$ films by altering the As defect structures [16]. Yet another source of compensation is Mn itself: the decrease in the magnitude of $\sigma_1(\omega)$ for $x > 0.052$ is a sign of the increasing importance of this channel of compensation at high Mn levels. In the subsequent analysis we will plot $\sigma_1^m(\omega) = \sigma_1^x(\omega) - \sigma_1^{x=1.7\%}(\omega)$, which simply has the effect of removing the high energy tail due to As antisites.

The frequency dependence of $\sigma_1(\omega)$ observed in Fig. 1 has a natural explanation within an impurity band model. In the very dilute doping limit, Mn forms an acceptor level 110 meV above the valence band [13,17]. Electronic transitions between this impurity level and the valence band produce a similar, but much weaker, resonance (dashed line in Fig. 1) than in ferromagnetic $\text{Ga}_{1-x}\text{Mn}_x\text{As}$. The

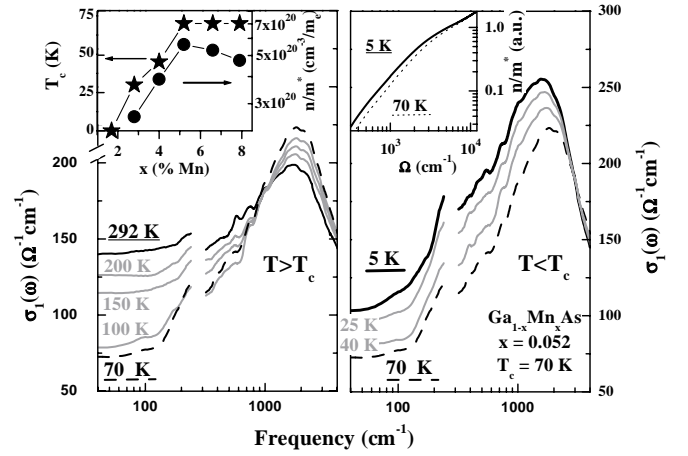


FIG. 2. Temperature dependence of $\sigma_1(\omega)$ for $x = 0.052$ sample on a log scale. Left panel shows $T \geq T_C$, while the right panel displays $T \leq T_C$. At temperatures above T_C all the spectra cross near 900 cm^{-1} . In contrast, below T_C no crossing is observed below 3000 cm^{-1} , indicating an overall increase in the low- ω spectral weight. Top left inset shows correlation between carrier density [Eq. (1)] at 292 K and T_C . Right inset demonstrates that the redistribution of spectral weight is confined to energies below 8000 cm^{-1} .

data for the ferromagnetic samples suggest that transitions from the valence band to Mn related electronic states may be the origin of this feature [18]. Interestingly, the native GaAs valence band structure provides an alternative source of this absorption. If the Fermi energy lies not within an impurity band, but in the GaAs valence bands, intervalence absorption processes may occur. Specifically, transitions are available between the heavy hole, light hole, and split off bands. Recent calculations suggest that both the expected energy and oscillator strength of these transitions are consistent with the resonance we observe in Fig. 1 [5].

While the frequency dependence of $\sigma_1(\omega)$ is consistent with both models, the effective mass m^* of the carriers is expected to be quite different within the valence band and impurity band scenarios of ferromagnetism. The magnitude of the effective mass can be estimated from the spectral weight, defined as

$$\frac{n}{m^*} = \frac{2}{\pi e^2} \int_0^{\Omega} \sigma_1(\omega) d\omega, \quad (1)$$

where n is the density of carriers, and Ω is a cutoff discussed below. In the valence band picture the entire spectrum of $\sigma_1^m(\omega)$ should be integrated, as the same bands are involved in the intraband and interband absorption processes [5]. For the impurity band case, only the oscillator strength of the intraband absorption is relevant for estimates of m^* . Therefore, the intraband and interband components must be separated. While no unique separation can be found from the data, by examining two extreme cases for this separation a range of likely masses may be inferred.

In the bottom panel of Fig. 1 we show two possible methods of extracting the intraband contribution of $\sigma_1(\omega)$. In the right panel we fit the data using the Drude-Lorentz model:

$$\sigma_1(\omega) = \frac{\omega^2}{4\pi} \sum_i \frac{\omega_{p,i}^2 \Gamma_i}{(\omega_{o,i}^2 - \omega^2)^2 + \omega^2 \Gamma_i^2}, \quad (2)$$

where $\omega_{p,i}^2$ is the strength of each oscillator, and Γ_i is the damping. The width of the Drude curve is chosen to be as wide as possible and still fit the data ($\Gamma_D = 6000 \text{ cm}^{-1}$). Since the height of conductivity spectrum is set by $\sigma_1(\omega \rightarrow 0)$, this yields the maximum possible spectral weight in the intraband channel. The left panel shows the opposite extreme, where the spectral weight of the intraband component is minimized. Here a single Lorentz oscillator (dashed line) is used to fit the absorption peak. This calculation is then subtracted from the data leaving the free carrier component shown with a thick line. Assuming that the carrier density is equal to the Mn concentration, integration of the data in the left panel of Fig. 1 where the spectral weight is the smallest yields a value of $m^* = 44m_e$ for the $x = 0.052$ sample. On the other extreme of high spectral weight we obtain $m^* = 2.1m_e$ for the same sample [19]. For the valence band picture where we simply integrate the experimental $\sigma_1^m(\omega)$, a value $m^* = 2.1m_e$ is also obtained [20]. Compensation is known to be strong in these materials and will reduce our estimates of the mass. High field Hall measurements report that hole doping is only a third of the Mn concentration [21]. Incorporating this estimate of compensation yields values of $15m_e$ and $0.7m_e$, respectively. These results favor a picture of the electronic structure involving impurity states at E_F , rather than that of holes doped into an unaltered GaAs valence band. Theoretical estimates of the mass of a 5% sample in the valence band scenario produce $m_B = 0.24m_e$ [5]. Such predictions could be reconciled with $m^* \geq 0.7m_e$ if other factors such as mass renormalization due to lattice and/or magnetic polarons are relevant.

The temperature dependence of m^* provides further insight into the origins of ferromagnetism in this system. In Fig. 2 we show the conductivity spectra at several temperatures above and below T_C . The left panel corresponds to temperatures $T \geq T_C$, while the right panel shows data at T_C and below. As the temperature is lowered from 292 K to T_C , the peak near 2000 cm^{-1} grows, while concomitantly $\sigma_1(\omega)$ is depressed at $\omega < 900 \text{ cm}^{-1}$. Importantly, there is a transfer of spectral weight [area under $\sigma_1(\omega)$] from low frequencies to the region near the peak as the temperature is lowered, so that there is an isosbestic point near 900 cm^{-1} . This should be contrasted with the behavior of $\sigma_1(\omega)$ below T_C , shown in the right panel. As the temperature decreases below T_C the peak maximum continues to increase, but at the same time $\sigma_1(\omega)$ at low frequencies *increases*, in contrast to the trend observed in the left panel. Notice that the spectra measured at $T < T_C$

in this energy range do not cross, which indicates that there is an overall increase in low frequency spectral weight.

The source of this increase in spectral weight below T_C can be understood in terms of a decrease of the effective carrier mass. In order to quantify this effect, we separate the intraband and interband components, as discussed previously. Figure 3 shows the temperature dependence of $\delta(n/m^*) = (n/m^*)_T - (n/m^*)_{T_C}$ for $T < T_C$ of the $x = 0.052$ sample, corresponding to the two extreme separation techniques shown in Fig. 1, and additionally from simply integrating the entire conductivity spectrum up to 4000 cm^{-1} . Below the ferromagnetic transition, $\delta(n/m^*)$, rises sharply. Regardless of the method used, the results reveal the same trend. Also plotted is the sample magnetization. The gain in low energy spectral weight closely tracks the magnetization. In other carrier mediated ferromagnets, such as the manganites[22] and more recently the hexaborides[23], a similar reduction of the itinerant carrier effective mass is observed below the ferromagnetic transition. Quite generally, a decrease in quasiparticle kinetic

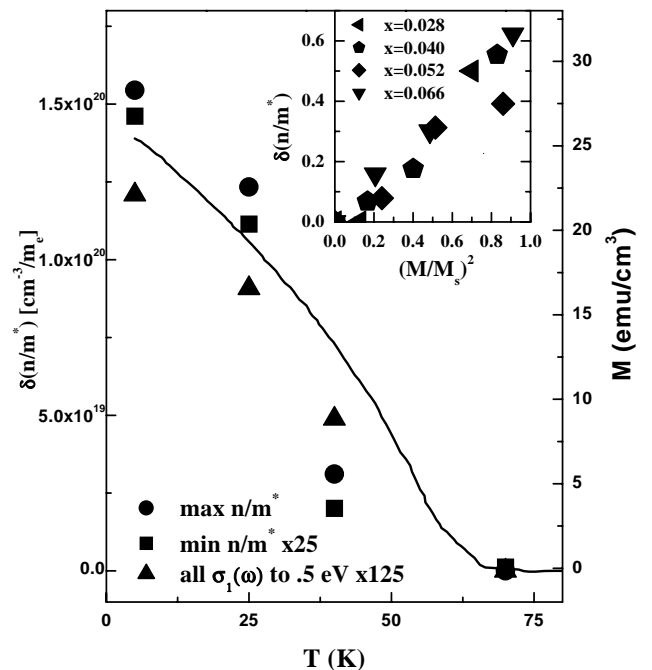


FIG. 3. Change in n/m^* below T_C calculated using both the maximum and minimum intraband spectral weight (Fig. 1), and from simply integrating the entire $\sigma_1(\omega)$ spectrum to 4000 cm^{-1} , for the $x = 0.052$ sample. Below T_C , the magnitude of n/m^* increases strongly with decreasing temperature. This increase of spectral weight can be interpreted in terms of a lowering of the charge carrier effective mass in the ferromagnetic state. The strong increase in n/m^* is observed in all samples, regardless of the method used to determine the intraband conductivity. Inset: Scaling relation between $\delta(n/m^*)$, normalized to the value of n/m^* at T_C , and the magnetization squared.

energy, proportional to n/m^* , has been proposed to drive the transition to the ferromagnetic state [24].

The correlation between magnetization and the large changes in the low energy spectral weight can be seen for several different Mn dopings in the inset of Fig. 3. Here we plot $\delta(n/m^*)$, normalized to the absolute value of the spectral weight at T_C , against the magnetization squared for all ferromagnetic samples. A single linear relation is observed for all the data regardless of T_C or Mn concentration. Such a scaling relation is expected within the double exchange model [25], and has been observed in the manganites [22]. This correlation between the magnitude of the carrier mass and magnetization is a further realization of the effects of carrier mediated ferromagnetism, which can also be seen in the doping dependence of T_C (left inset of Fig. 2).

The large values obtained for the effective mass ($0.7m_e < m^* < 15m_e$) and the decrease in the magnitude observed below T_C can both be explained within the impurity band picture. The relatively small width of an impurity band will give rise to a mass enhanced above the free electron value. Additionally, a decrease in band mass can occur below T_C for itinerant carriers in a narrow band [22]. Alternatively, the interpretation of the magnitude and temperature dependence of the effective mass is less clear in the picture of holes doped into the GaAs valence band.

An important issue to address in the sum rule analysis is the energy scale involved in the redistribution of spectral weight at $T < T_C$. From the global oscillator strength sum rule, $\frac{n}{m_e} = \frac{2}{\pi e^2} \int_0^\infty \sigma_1(\omega) d\omega$, one expects that the gain in low energy spectral weight below T_C must be compensated by a decrease in spectral weight at higher ω . This energy scale holds important information about the strength of the magnetic exchange interaction. The inset of the right panel of Fig. 2 shows n/m^* as a function of cutoff frequency, Ω , for the $x = 0.052$ sample at 5 K and T_C . At low energies the 5 K curve is enhanced above the value at T_C . However, by 8000 cm^{-1} the spectral weight is independent of temperature. The low energy spectral weight actually begins to be recovered at $\omega \sim 3000 \text{ cm}^{-1}$ where the 70 K, $\sigma_1(\omega)$ curve crosses above the 5 K spectrum. This should be contrasted to other systems like the manganites, where the low energy spectral weight lost below T_C is not recovered until $\omega \sim 2-3 \text{ eV}$, on the order of the Hund's coupling exchange energy [22]. The Mn ion in $\text{Ga}_{1-x}\text{Mn}_x\text{As}$ is in the d^5 state [17,26], so here the large Hund's coupling will not be the relevant exchange energy. Rather a much smaller kinetic exchange term should dominate [3]. Indeed, the crossing of the conductivity curves at $\omega \sim 3000 \text{ cm}^{-1}$, and the complete exhaustion of the sum rule by $\omega \leq 8000 \text{ cm}^{-1}$ (1 eV) is consistent with a lower energy exchange coupling in this system.

In summary, a strong midinfrared absorption band is observed in all ferromagnetic samples of $\text{Ga}_{1-x}\text{Mn}_x\text{As}$. While both impurity band absorption and intervalence transitions can describe this feature, a sum rule analysis suggests the carriers are heavier than expected for holes doped into the unperturbed GaAs valence band. The strong enhancement of the low- ω spectral weight at $T < T_C$ is a direct result of the reduction in mass of the heavy carriers which drives the ferromagnetic transition.

The authors thank L. Sham, A. MacDonald, J. Fernandez, T. Jungwirth, and J. Sinova for helpful discussion. This work was supported by the DOE, NSF, DARPA, and ONR.

-
- [1] H. Ohno, *Science* **281**, 251 (2001).
 - [2] S. A. Wolf *et al.*, *Science* **294**, 1488 (2001).
 - [3] F. Matsukura *et al.*, *Phys. Rev. B* **57**, 2037 (1998).
 - [4] J. Szczytko *et al.*, *Phys. Rev. B* **59**, 12935 (1999); B. Beschoten *et al.*, *Phys. Rev. Lett.* **83**, 3073 (1999).
 - [5] J. Sinova *et al.*, cond-mat/0204209 (unpublished).
 - [6] J. König *et al.*, *Phys. Rev. Lett.* **84**, 5628 (2000).
 - [7] G. Zarand and B. Janko, cond-mat/0108477 (unpublished).
 - [8] J. Okabayashi *et al.*, *Phys. Rev. B* **64**, 125304 (2001); H. Asklund *et al.*, cond-mat/0112287 (unpublished).
 - [9] Y. Nagai *et al.*, *Jpn. Soc. Appl. Phys.* **11**, 6231 (2001).
 - [10] H. Akai, *Phys. Rev. Lett.* **81**, 3002 (1998); T. Dietl *et al.*, *Science* **287**, 1019 (2000); J. Inoue *et al.*, *Phys. Rev. Lett.* **85**, 4610 (2000); D. E. Angelescu and R. N. Bhatt, *Phys. Rev. B* **65**, 075211 (2002); S. Sanvito *et al.*, *Phys. Rev. B* **63**, 165206 (2001).
 - [11] H. Ohno, A. Shen, F. Matsukura, A. Oiwa, A. Endo, S. Katsumoto, and Y. Iye, *Appl. Phys. Lett.* **69**, 363 (1996).
 - [12] E.J. Singley *et al.* (unpublished).
 - [13] R. A. Chapman and W. G. Hutchinson, *Phys. Rev. Lett.* **18**, 443 (1967).
 - [14] M. O. Manasreh *et al.*, *Phys. Rev. B* **41**, 10272 (1990).
 - [15] D. C. Look *et al.*, *Phys. Rev. B* **42**, 3578 (1990).
 - [16] S. J. Potashnik *et al.*, *Appl. Phys. Lett.* **79**, 1495 (2001).
 - [17] M. Linnarsson *et al.*, *Phys. Rev. B* **55**, 6938 (1997).
 - [18] E. H. Hwang *et al.*, cond-mat/0202071 (unpublished).
 - [19] All other dopings had larger masses (up to 60% greater).
 - [20] These two values can be the same since the broad Drude model includes a substantial amount of spectral weight in the tail which is outside of our experimental range.
 - [21] H. Ohno *et al.*, *J. Appl. Phys.* **85**, 4277 (1999).
 - [22] Y. Okimoto *et al.*, *Phys. Rev. B* **55**, 4206 (1997); K. H. Kim *et al.*, *Phys. Rev. Lett.* **81**, 4983 (1998); T. Ishikawa *et al.*, *Phys. Rev. B* **57**, 8079 (1998).
 - [23] S. Broderick *et al.*, *Phys. Rev. B* **65**, 121102 (2002).
 - [24] J. E. Hirsch, *Phys. Rev. B* **62**, 14131 (2000).
 - [25] N. Furukawa, *J. Phys. Soc. Jpn.* **63**, 3214 (1994).
 - [26] J. Schneider *et al.*, *Phys. Rev. Lett.* **59**, 240 (1987).